Biomedical Research and Therapy 2024, 11(5):6402-6420

Open Access Full Text Article

Research Article

Development of a 3D-printed negative pressure cutter for precise apical resection in neonatal mouse hearts

Minh-Thu Le[1,2], Thi-Thu-Hien Pham[1,2], Thanh-Hai Le[3], Quoc-Hung Phan[4], Van-Toi Vo[1,2], Ngoc-Bich Le[1,2,*]

ABSTRACT

Introduction: The cardiac cells of neonatal mice, only one day old, exhibit ongoing cell cycle activity for a duration of 14 days following parturition. Their hearts have a strong capacity to replace cardiomyocytes, which disappears in adulthood, in order to respond to injuries sustained during that time. Numerous studies have been conducted to examine the intrinsic regenerative capacity of neonatal mice's hearts following a resection of 1 millimeter from the ventricular apex. However, it should be noted that there is currently a lack of specialized cutting tools designed specifically for this particular field of research. This absence of appropriate instruments may result in challenges when attempting to achieve consistent sample cuts, as human error can introduce variability. Furthermore, it is important to acknowledge that larger cuts may pose a significant risk to the subject's life. **Methods**: This project involved the fabrication of a 3D-printed cutter utilizing a negative pressure system. The surgical scalpel blade is affixed to the cutter, enabling the automated removal of the apex from the heart to the desired diameter, without the need for manual measurements. The cutter underwent multiple iterations and adjustments prior to reaching its final configuration, resulting in the inclusion of numerous variables in the subsequent tests. Furthermore, due to temporal constraints, the final experiment is limited to a relatively small sample size of 16 subjects. **Results**: The dataset obtained from the experiment was examined in order to draw a conclusion. It was found that the removal with the cutter has resulted in a relatively stable diameter. However, the size of the resection is still slightly greater than 1 millimeter, indicating that it has not yet reached the intended dimension initially desired. **Conclusion**: The innovative 3D-printed negative pressure cutter provides a more efficient and automated method for precise apical resection in neonatal mouse hearts, overcoming the drawbacks of manual procedures and variability in sample cuts. This study represents an initial endeavor towards refining the cutter for apical resection in the hearts of neonatal mice, thereby laying the foundation for future advancements in this field.

Key words: Apical resection, cardiac apex, negative pressure cutter, surgical scalpel blade, 3D printin

[1]*School of Biomedical Engineering, International University, Ho Chi Minh City 700000, Viet Nam*

[2]*Vietnam National University HCMC, Ho Chi Minh City 700000, Viet Nam*

[3]*Department of Information Technology Specialization, FPT University, Ho Chi Minh City 700000, Viet Nam*

[4]*Department of Mechanical Engineering, National United University, Miaoli 360302, Taiwan*

Correspondence

Ngoc-Bich Le, School of Biomedical Engineering, International University, Ho Chi Minh City 700000, Viet Nam

Vietnam National University HCMC, Ho Chi Minh City 700000, Viet Nam

Email: lnbich@hcmiu.edu.vn

History

- Received: Jan 01, 2024
- Accepted: Mar 14, 2024
- Published Online: May 31, 2024

DOI : 10.15419/bmrat.v11i5.886

INTRODUCTION

Following a myocardial infarction, a considerable number of cardiomyocytes may undergo irreversible loss, as the regenerative capacity of adult hearts to generate new cardiac muscle cells is inadequate [1]. The implementation of regenerative technologies in the context of cardiac rehabilitation has been identified as a feasible strategy for the treatment of heart failure [2–16]. The initial investigations into cardiac regeneration were carried out on amphibians [17] and newts [18]. The discovery of evidence regarding the cardiac regenerative capacity of mammals occurred only within the past decade [19]. An intriguing characteristic was discovered during a study on the cardiac regeneration of rodents: in the event that cytokinesis is not present, rodent cardiomyocytes undergo a final round of DNA synthesis and karyokinesis, leading to the binucleation of approximately 90-95% of cardiomyocytes by postnatal day 14 [20,21]. According to Kikuchi and Poss (2012) [22], a significant proportion of mammalian cardiomyocytes undergo permanent cell cycle arrest prior to reaching adulthood. The absence of a robust proliferative response in non-regenerative adult mammals is a significant characteristic of cardiac regeneration in neonatal mice that are one day old [23].

The neonatal mouse has been identified as a highly suitable mammalian model for investigating the mechanisms underlying mammalian heart regeneration [24–33]. This is primarily due to its remarkable ability to completely regenerate its heart within a period of 21 days following apical resection [34]. During the investigation of this subject matter, a segment of the ventricular apex is excised for the purpose of assessing and contrasting the regenerative capabilities

BioMedPress
The Open Access Publisher

Cite this article : Le M, Pham T, Le T, Phan Q, Vo V, Le N. **Development of a 3D-printed negative pressure cutter for precise apical resection in neonatal mouse hearts**. *Biomed. Res. Ther.* 2024; 11(5):6402-6420.

across various subjects[35,36]. However, the cuts are not consistent, resulting in challenges when attempting to make comparisons. According to a study conducted by Li *et al.* (2020)[35], certain extensive resections have the potential to result in the mortality of the animal.

The mouse heart, similar to numerous mammals, is enveloped by the pericardium, a dual-layered structure containing pericardial fluid[37]. The primary role of this layer is to protect the heart from infection and to prevent excessive dilation of the heart[38]. According to Jaworska-Wilczynska *et al.* (2016)[38], the function of the pericardial fluid is to provide lubrication to the heart, thereby minimizing friction during its operation. The pericardium is composed of resilient connective tissue that exhibits high resistance to rupture, effectively fulfilling its functional role.

The presence of this protective layer impedes the process of heart resection. During the cutting procedure, the flexible pericardium has the potential to alter the trajectory of the incision, thereby introducing additional complexities to the aortic valve replacement (AR) procedure.

Effective apical excision in newborn mouse hearts could enhance our understanding of cardiac regeneration mechanisms and guide the creation of regenerative treatments for heart disease. Precise apical resection techniques can impact surgical interventions in human patients by providing opportunities for minimally invasive procedures and better patient outcomes.

According to Li *et al.* (2020)[35], the current method for conducting apical resection involves the use of a thoracotomy incision measuring 1 cm in length, which allows for visualization of the heart's location. The apex is securely held in place using microsurgical tweezers, and a tiny portion is excised from the apex through a single incision made with a pair of iridectomy scissors[39,40].

In another investigation, Xiong and Hou employed iridectomy spring scissors to create an incision in the cardiac apex following the thoracotomy procedure[32]. The apical resection was performed in a stepwise manner through the implementation of multiple incisions prior to the complete excision of a portion of the cardiac apex[32].

The case studies examined demonstrate that the entire process is carried out manually by individuals, without the involvement of any automated systems. Consequently, this manual execution leads to variations in the sizes of the cuts. According to a study conducted by Li *et al.* (2020)[35], resections that result in an exposure exceeding 1.5 millimeters could potentially impact the rate of heart regeneration and potentially lead to fatality in certain circumstances.

The primary aim of this study is to develop a precise incision on the apex of the heart, ensuring a diameter within a range of 1 millimeter. The consideration of speed is also pertinent, as a high-speed cut can effectively reduce inaccuracies resulting from the pericardium. Furthermore, the resection should not cause any heat burn as these factors are not included in the study of cardiac rehabilitation.

METHODS

Design

Expected specifications and features

Table 1 summarizes the expected specifications and features that must be considered during device design. The expected characteristics include using neonatal murine cardiac tissue as experimental specimens, a circular cutting specimen with polished boundaries, a cutting sample diameter of 1 millimeter, a level and uncontaminated resected surface, and an automated operational procedure with a high cutting velocity. Furthermore, it is imperative to consider several crucial inquiries to guarantee the successful development of the apparatus: (i) What measures can be taken to ensure the secure fixation of the apex of the heart during the cutting process? (ii) What strategies can be implemented to guarantee uniform sample diameters during the resection process? (iii) Which blade shape would be the most appropriate choice for the project? What is the most effective technique for executing the incision to maximize the excision? What strategies can be employed to mitigate human error during the resection process?

Figure 1 shows the research framework, serving as a visual representation of our methodology and facilitating the understanding of the workflow followed in our research. The diagram provides a comprehensive overview of the research process from device design to experimental testing and results analysis. The graphic illustrates two methods to stabilize the apex: clamping or negative pressure. However, clamping alone does not guarantee consistent sample shape and diameter measurements. Conversely, a circular tube connected to a negative pressure system creates a consistent "framework" around the heart's precise cutting site, allowing the blade to penetrate and maintain consistent size.

To select the right cutting blade and perform the best resection, a research study on blade forms is required.

Table 1: Engineering goal specification

Specification	Requirement
Research subject	Neonatal mice heart
Shape of the cutting sample	Round with smooth edge
Size of the cutting sample	1 millimeter in diameter
Resected surface	Flat and clean
Operation	Automated High cutting speed
Place of use	Laboratory
Portability	Compact, lightweight, portable design

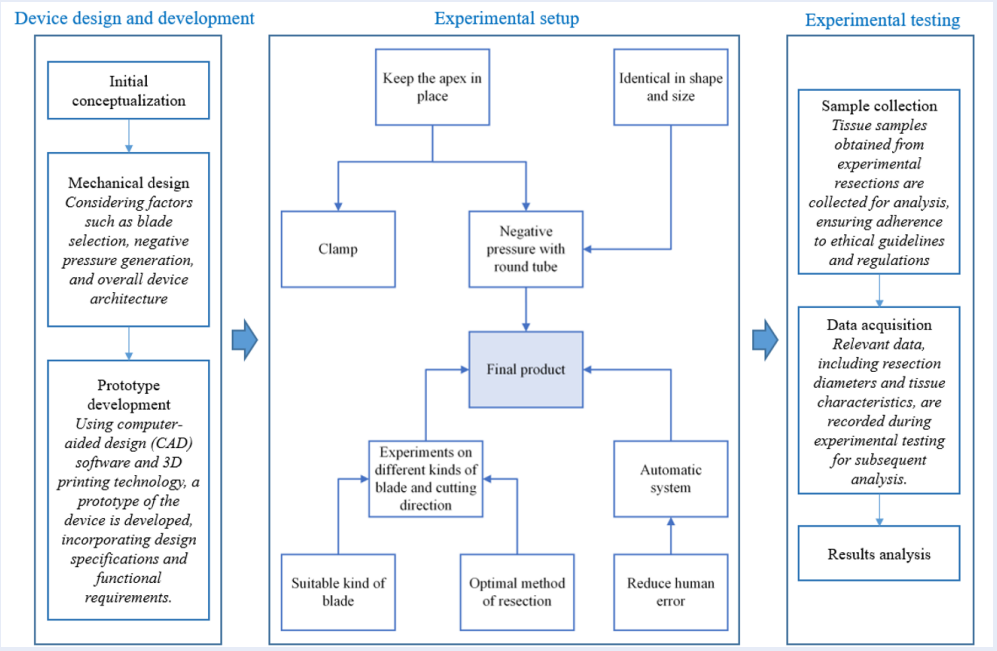

Figure 1: Demonstration of the research process including (1) device design and development, (2) experimental setup, and (3) experimental testing and results analysis.

Experiments on blade positioning are necessary to establish the best resection procedure.

In order to mitigate potential human errors during experimental procedures, it is advisable to implement an automated cutting system. The design of the system should incorporate a mechanism that initiates the entire system when a predetermined element is activated, thereby ensuring the system's automatic operation. By integrating an automated system, the likelihood of human error can be significantly reduced.

Mechanical design

Figure 2 displays the functional concept design of the proposed device, demonstrating its numerous features that ensure uniform and consistent resections. An automated cutting mechanism and a negative pressure system are crucial to the design. The practical concept design employs a suction head to control the size of incisions. The suction head and negative pressure system work in tandem to maintain the heart apex in position during cutting. This gadget utilizes a negative pressure system to minimize cardiac apex movement, thereby enhancing the precision of resections.

Figure 3A illustrates the device's main body, trigger, latch, and cutter. These components collaborate to automate the cutting process. The framework offers stability and supports the apparatus's various mech-

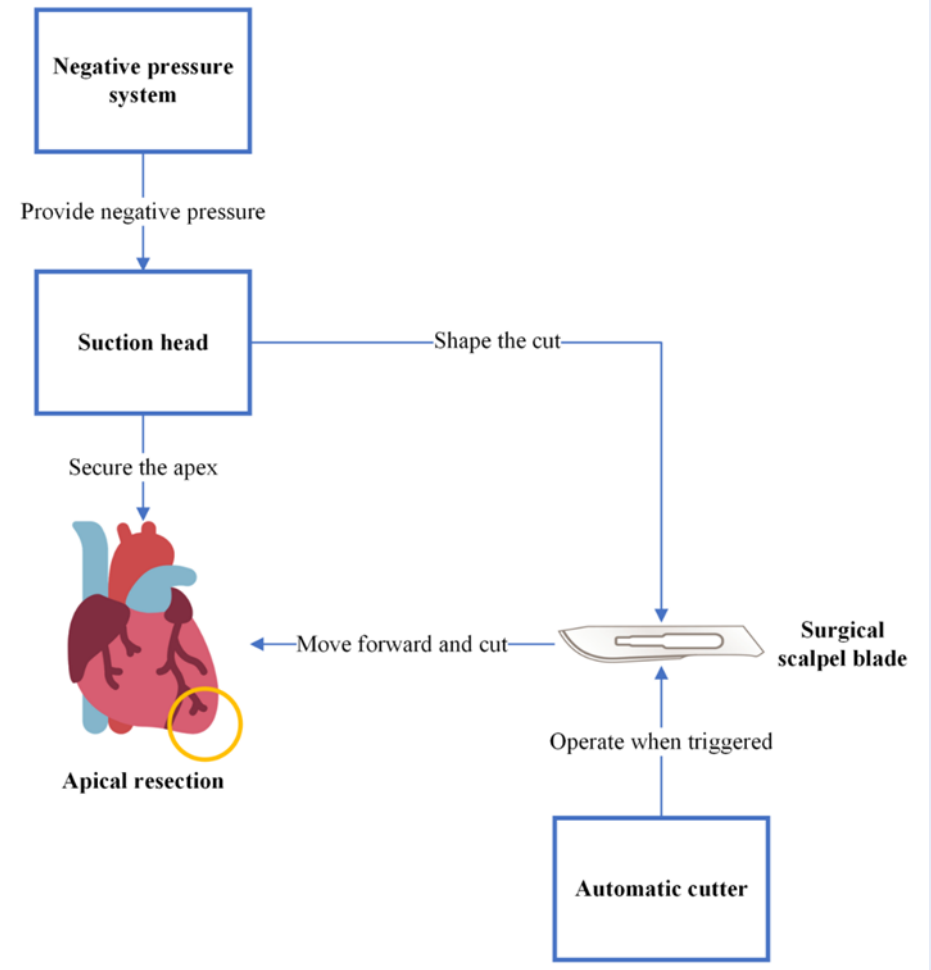

Figure 2: **Correlations between the functional blocks: The negative pressure system provides negative pressure to the suction head to secure the apex, and the automatic cutter utilizes spring actuation and trigger mechanism to move the surgical scalpel blade at high speed to produce the cutting operation on the secured apex**.

anisms. The trigger mechanism initiates the cutting operation, while the latch mechanism secures the cutter in place throughout the resection. The cutter, being the main component, performs precise cuts. **Figure 3B** reveals the device's complete structural design and component configuration. This visual representation demonstrates how the main body, trigger, latch, and cutting components are combined into a functional device.

Figure 2 and **Figure 3** highlight the device's innovative features and mechanisms, emphasizing the automation of the cutter and the critical role of the negative pressure system in ensuring resection precision and uniformity.

The main body design

Figure 4 provides a visual representation of the main frame of the device, which acts as the central component responsible for integrating and connecting the diverse elements into a cohesive and operational entity. The main body of the apparatus encompasses several essential components, namely: (i) the sliding slot (a), (ii) the spring position (b), (iii) the fulcrum for the trigger mechanism, (iv) the fixation points for the tube, (v) the knobs situated on both sides, and (vi) the designated position for the suction head. The sliding slot (a) plays a crucial role in facilitating the seamless movement of specific components within the device, thereby enabling the automated cutting process. The spring position (b) refers to the precise placement of the spring within the device, which plays a role in

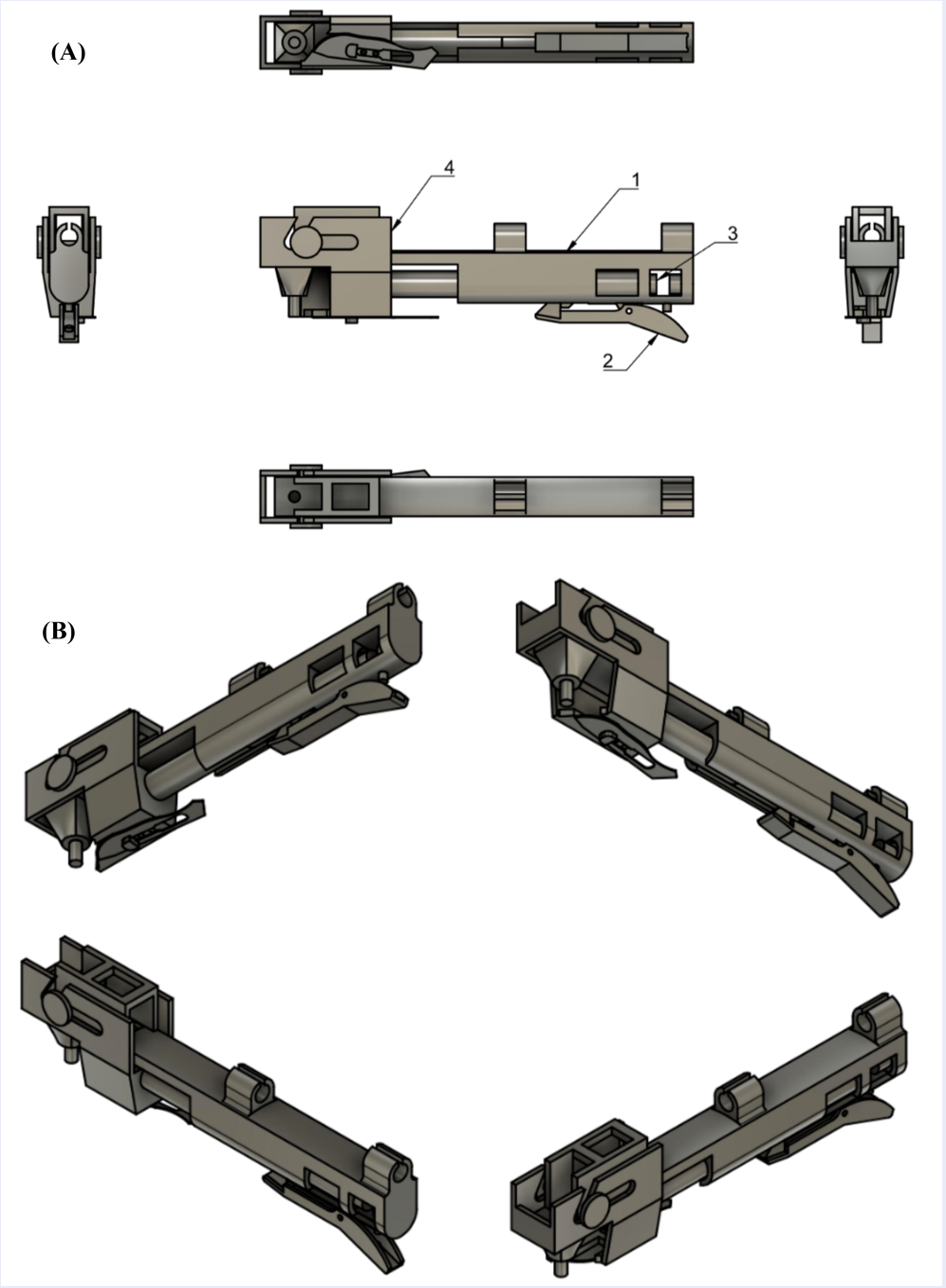

Figure 3: **Demonstration of different views of the 3D design including (A) front, top, bottom, and side views, and (B) different perspective views.**

determining its overall functionality. The fulcrum, also referred to as the pivot point, plays a crucial role in guaranteeing the efficient functionality of the trigger mechanism. The fulcrum serves as a pivotal point for the trigger, facilitating the initiation of the cutting mechanism. The air pipeline is guided along the length of the main body by two fixation points consisting of tubes. The inclusion of this feature is essential for facilitating the optimal circulation of air within the device, thereby playing a crucial role in its overall operational effectiveness. The inclusion of knobs on both sides of the main frame provides ergonomic advantages, enabling convenient manipulation and regulation during usage. Furthermore, the designation of the suction head position refers to the precise location at which the inlet of the scalp vein set is securely affixed. The positioning of this component guarantees a reliable and consistent linkage between the suction head and the vein set, thereby facilitating the optimal functioning of the negative pressure system.

Figure 5 presents a detailed illustration that elucidates the precise measurements and dimensions of the main body's structure, thereby enhancing the comprehensiveness of understanding. This comprehensive architectural illustration functions as a valuable point of reference, facilitating the precise construction and integration of the apparatus. The analysis and discussion of the main body's characteristics, as depicted in **Figure 4** and **Figure 5**, shed light on the critical components and design considerations involved in developing a functional and effective device for the intended application.

The cutter design

In **Figure 6**, the cutter's cutting frame is detailed. The cutter secures the scalpel blade. The sliding slot (a) and two knobs secure the item to its main body. The cutting device's cylindrical arm moves within the main frame's sliding slot (a). The current design facilitates precise placement of the cutting tool throughout the process. The sliding slots (b), with an acute angle of 60 degrees, allow for smooth movement of the cutter along the main body's knobs. This mechanism ensures cutting precision and stability. Two pairs of M2 screws and nuts secure the scalpel blade to the underside of the cutter. This fastening mechanism maintains the blade's stability and alignment throughout the cutting process. Detailed measurements and dimensions of the cutting frame are presented in **Figure 7**, elucidating its structure and size. The detailed structural schematic assists in the fabrication and assembly of the cutting frame, ensuring accuracy and precision.

Figure 6 and **Figure 7** depict the cutter's structural configuration, elucidating its components and their functions. This analysis explores the connections between the cutter, main body, and scalpel blade, highlighting the complex design principles necessary to create an efficient and reliable cutting process. Surgical blades are used for maximum quality. The cutter must be sharp enough to pierce tissue. Stainless steel scalpels are available for single-use disposal or multiple uses. Reusable scalpels may have detachable blades or permanently attached blades that can be sharpened. Each single-use scalpel blade has a numerical identifier based on its shape and size. Blade sizes #10, #11, #12, and #20 are prevalent in Vietnamese medical equipment retailers (**Figure 8**). All pieces are made of stainless steel and feature two ground-edge designs. The cutter's forward action limits its compatibility to diagonal cutting blades, such as the #11, or outward-curving blades like the #10 and #20. After testing, the #20 scalpel blade outperforms the other two. Blade #10 was too small for the cutter. The scalpel blade #11's straight cutting edge tends to detach from the heart apex, hindering incisions.

The Latch Design

Figure 9 illustrates the structure of the latch mechanism. The latch features a cylindrical tube with the same diameter as the cutter's arm. This design extends the arm, facilitating spring compression. A latch is affixed to the cylindrical tube structure to ensure optimal performance. This latch is inserted into the sliding chamber of the main body to connect with the trigger mechanism and compress the spring as required. The latch and the main body's spring positions (a) are linked by a 10 mm metal spring. This spring compresses and secures the spring position, aiding the latch mechanism's functionality.

Figure 9 provides a detailed view of the latch's design and structure. The figure highlights a 2.4-millimeter aperture that connects the cutting tool's "male" component. The latch also features a 2.7-millimeter section for D2 magnets, guaranteeing a robust connection with the cutter.

Figure 9 and **Figure 10** exhibit the latch mechanism's intricate components and design elements. This analysis delves into the round tube structure, latch attachment, spring positioning, and joint securing mechanisms to gain a deeper comprehension of how the latch supports the cutting mechanism's operation and synchronization.

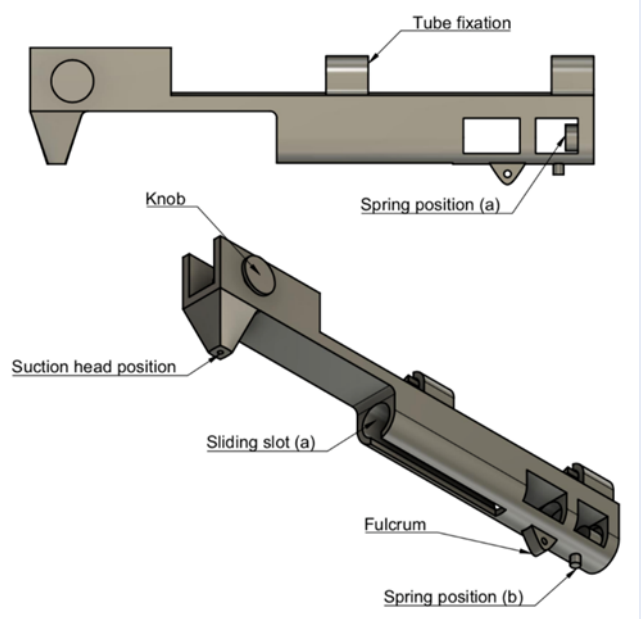

Figure 4: **A graphical depiction of the device's main frame with various vital elements (i) the sliding slot (a), (ii) the spring position (a), (iii) the fulcrum for the trigger mechanism, (iv) the fixation points for the tube, (v) the knobs situated on both sides and (vi) the designated position for the suction head.**

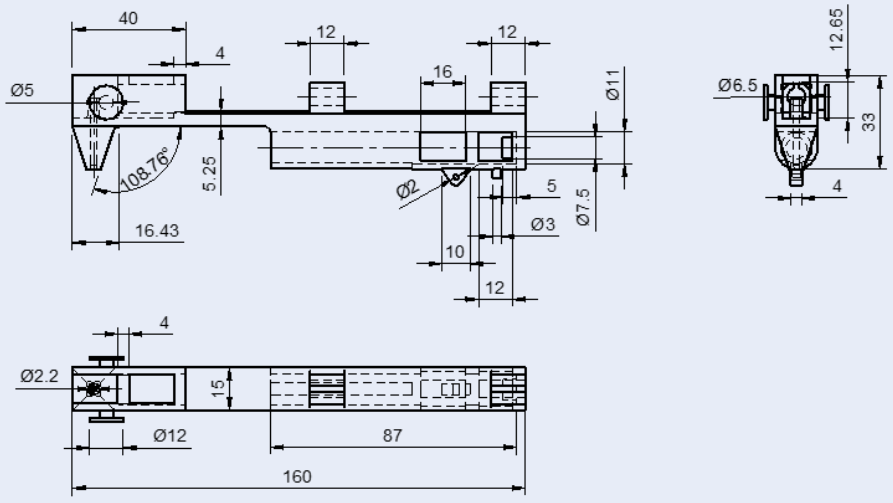

Figure 5: **Front, Top, and Side views 2D design with detailed dimensions of the main body. The boundary dimensions are about 160mm x 20mm x 40mm.**

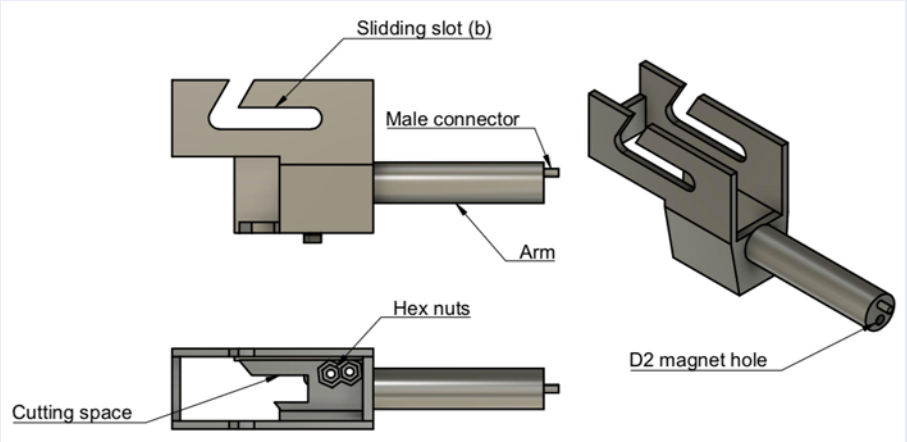

Figure 6: **Front, Top, and Perspective views to illustrate the structural design of the cutting frame with sliding slot (b) with an acute angle of 60º, cutting space, M2 hex nuts to secure the cutting blade, cylindrical arm moving in the main frame's sliding slot (a), male connector and D2 magnet hole.**

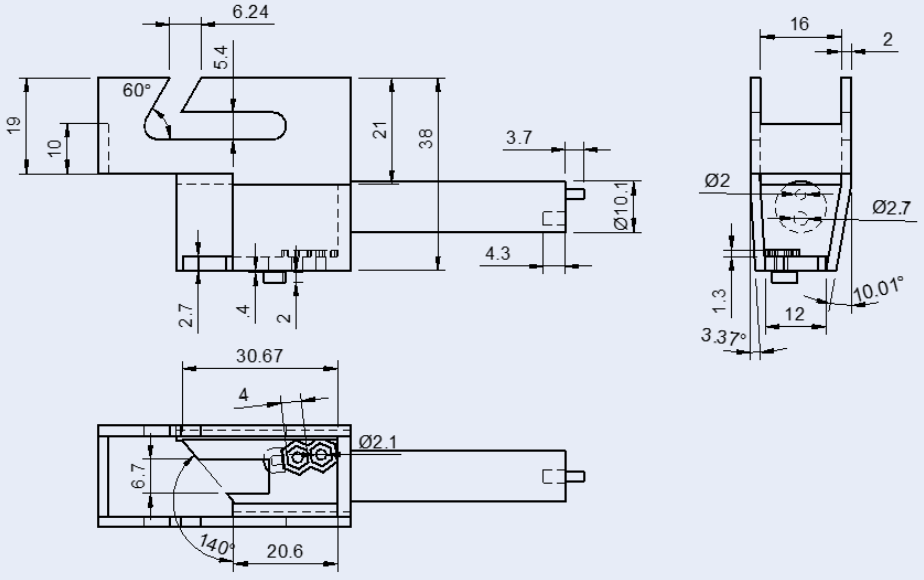

Figure 7: **Front, Top, and Side views 2D design with detailed dimensions of the cutting frame.** Overall sizes are about 90 mm x 20 mm x 40 mm.

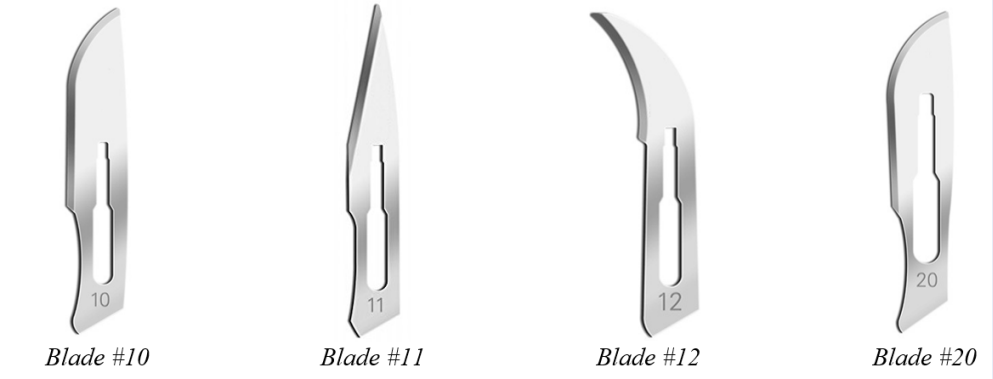

Figure 8: **Visual demonstration of different surgical scalpel blades. Blade sizes #10, #11, #12, and #20**. Each item is crafted from stainless steel and features two ground-edge designs.

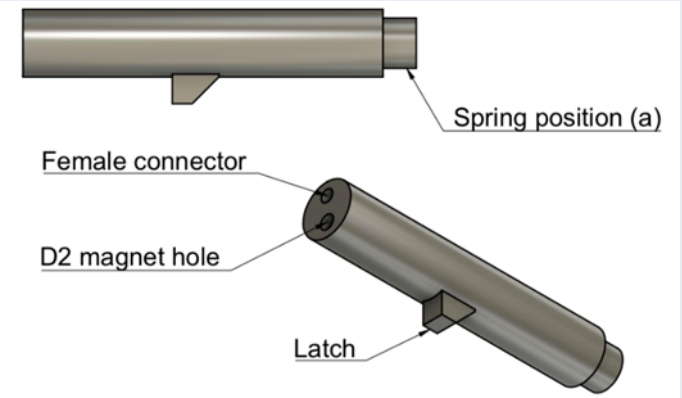

Figure 9: **Top and perspective illustration of the latch mechanism's structure**. By insertion into the sliding chamber of the main body, this latch establishes a connection with the trigger mechanism and, when necessary, compresses the spring. 10 mm diameter metal spring is utilized.

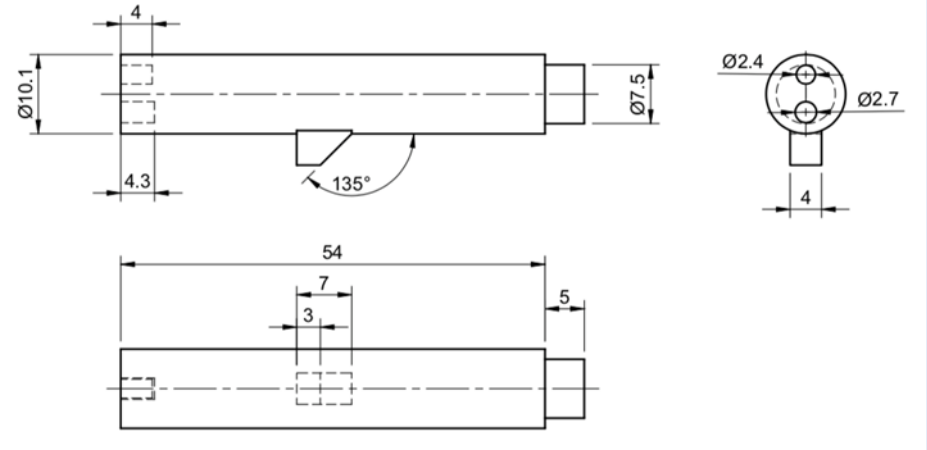

Figure 10: **Front, Top, and Side views 2D design with detailed dimensions of the latch**. The main arm's cylindrical diameter is 10.1 mm, total length is 59 mm.

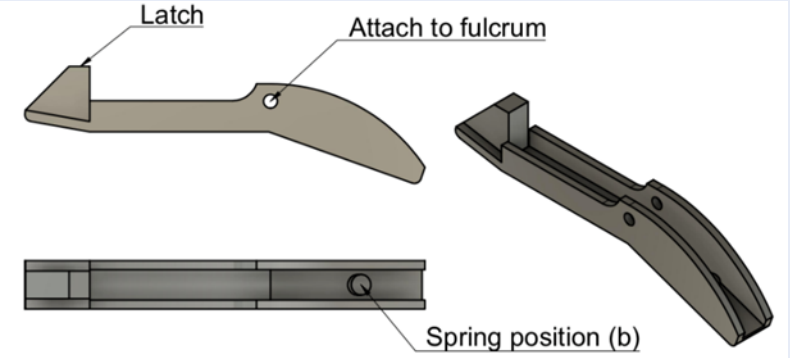

Figure 11: **Front, Top, and Perspective views to illustrate the structural design of the trigger with latch, position to attach to the fulcrum, and spring position (b). A 5 mm diameter, 15 mm free length spring links the main body and trigger spring positions (b).**

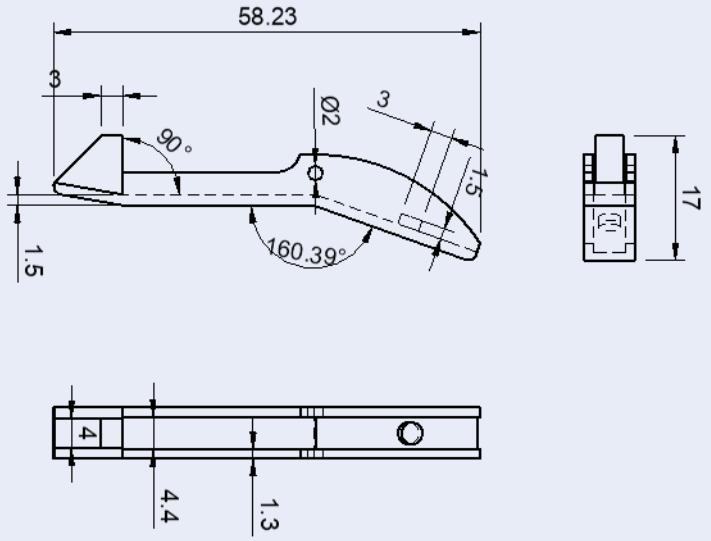

Figure 12: **Front, Top, and Side views 2D design with detailed dimensions of the trigger**. Overall dimensions are roughly 58 mm x 4 mm x 17 mm, bending angle is about 160 degrees.

The Trigger Design

Figure 11 illustrates the 3D visualization, and **Figure 12** shows the detailed structure and dimensions of the trigger's Class 2 lever mechanism, as described by Davidovits in 2008[41]. The fulcrum is attached to the main frame, and the spring loads the arm downward. The force-applying point is located farther from the fulcrum than the spring. This arrangement increases mechanical advantage, allowing users to initiate movements with less force. The arm is flexed at the fulcrum to maintain parallel alignment between the latch-holding part and the main body during inactivity. When compressed, the trigger latch aligns precisely with the latch design because it is parallel to the main body (**Figure 14A**). A 5 mm spring connects the main body and the trigger spring positions (**Figure 14B**). Two metal springs were utilized in this study. The larger one has a 10 mm inner diameter, 50 mm length, and 0.3 mm wire diameter. The smaller one has a 0.5 mm wire diameter, 5 mm diameter, and 15 mm free length.

Negative Pressure Generation

A negative pressure generator is crucial for building a system. Therefore, the selection of the best pressure generator takes into careful consideration the pressure range, the capacity to maintain pressure, the

power supply, and mobility. **Figure 13** illustrates a small air pump used to create negative pressure. Utilizing a regulating valve to maintain a steady negative pressure stabilizes the sample and facilitates easier and more uniform resection. Micro air pumps, also known as diaphragm pumps or vacuum pumps, are compact, water-resistant pumps capable of generating high pressure. The device draws in air through an air inlet, thereby creating negative pressure. Air can also be expelled through its outlet. Both openings are compact, featuring a 4.2-millimeter outside diameter.

Experimental setup

Figure 14 illustrates the operational mechanism of the negative pressure cutter. When the apex of the heart is positioned at the suction head, negative pressure will draw it in and secure it in place; subsequently, (a) the cutter is pushed to the left into the compressed position. (b) The release of the latch occurs when force is applied to the trigger located at the arrow position. (c) The spring exerts force on the latch and the cutter, causing them to move in the leftward direction. (d) Subsequently, the trigger returns to its initial position at high velocity and performs the cutting.

The choice of a sample size of 16 participants was influenced by difficulties in obtaining appropriate samples and ethical concerns related to dealing with live animals. Obtaining neonatal mouse hearts for our research was challenging due to issues such as breeding schedules, housing constraints, and ethical regulations. The availability of neonatal mice within the necessary age range fluctuated, depending on breeding cycles and litter sizes. To maximize research efficiency, we sought to utilize the limited number of neonatal mouse hearts that met our specific requirements within a set timeframe. It is essential to find a balance between the ethical treatment of animals in research and the need to obtain statistically significant results.

RESULTS

Prototype and Cutting Results

Figure 15 illustrates the culmination of the design process, displaying the ultimate outcome of the proposed device. The diagram highlights several components, including the adapted scalp vein set, the air pipe, and the micro vacuum pump. The inclusion of these elements is crucial for ensuring the device's comprehensive functionality and optimal effectiveness.

The positioning of the suction head's inlet is a significant aspect of the finalized design. As the cutter moves forward, the suction head inlet comes into contact with the side of the scalpel blade, given that they are positioned parallel to each other. This arrangement ensures the optimal activation of the negative pressure system, effectively securing the tissue in place throughout the cutting process.

Figure 16 presents a visual depiction of cut samples derived from the experiment. These samples serve as concrete evidence of the device's performance and its ability to achieve precise and consistent cuts as per the intended specifications.

The outcomes depicted in **Figure 15** and **Figure 16** demonstrate the effective implementation of the design, showcasing the seamless integration of diverse components and their corresponding functionalities. The final product's incorporation of the modified scalp vein set, air pipeline, and micro vacuum pump exemplifies the device's proficiency in performing accurate incisions while maintaining tissue stability. Moreover, the exhibition of excised tissue specimens acts as a definitive illustration of the device's ability to produce reliable and uniform results, thus substantiating its suitability for implementation in research endeavors pertaining to apical resection in neonatal murine cardiac studies.

Data Analysis

The data were obtained from a total of 16 samples, each captured using a camera equipped with a calibration ruler for reference. The captured images were subsequently converted into a digital format. The computer was then used to analyze and measure the diameter of the samples. The data are visually represented by a histogram, as shown in **Figure 17**. According to the data presented in the graph, the mean value (\(\bar{x} \)) is observed to be 1.4736 millimeters, while the standard deviation (\(s \)) is measured at 0.306 millimeters. Utilizing the One-sample T-test to establish a 95% confidence interval for the difference, the lower bound is found to be 1.3106 millimeters, while the upper bound is 1.6367 millimeters.

The Q-Q plot in **Figure 18** illustrates the presence of skewness in the dataset. **Table 2** provides a more comprehensive depiction of the data distribution, with a skewness statistic of 0.563. This indicates that the distribution exhibits a moderate positive skew, suggesting a rightward skewness. The presence of skewness is also observable through the Q-Q plot. The kurtosis statistic is -0.550, indicating that the distribution has slightly lighter tails than a normal distribution. In other words, the kurtosis value signifies a slight deviation from normality.

Table 3 presents the results of applying the Shapiro-Wilk test in this specific context, with a sample size

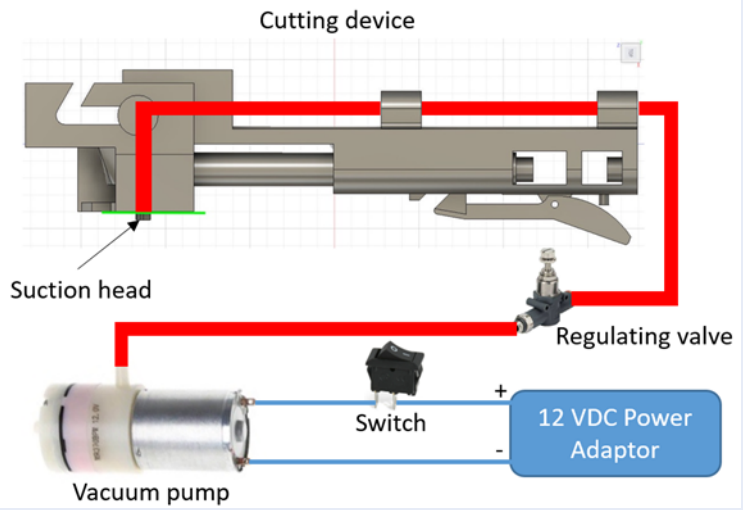

Figure 13: **Configuration of the pneumatic system including 12 VDC power adapter to supply power, switch to turn on and off the operation, vacuum pump to produce negative pressure, regulating valve to secure the pressure at a setting level, and suction head to secure the apex of the heart.**

Table 2: **Descriptive statistics**

		Statistic	Std. Error
Mean		1.47363	0.076490
95% Confidence Interval for Mean	Lower Bound	1.31059	
	Upper Bound	1.63666	
5% Trimmed Mean		1.46547	
Median		1.43750	
Variance		0.094	
Standard Deviation		0.305961	
Minimum		1.044	
Maximum		2.050	
Range		1.006	
Interquartile Range		0.484	
Skewness		0.563	0.564
Kurtosis		-0.550	1.091

Table 3: **Tests of normality**

	Shapiro – Wilk		
	Statistics	**df**	**Sig.**
Diameter	0.949	16	0.474

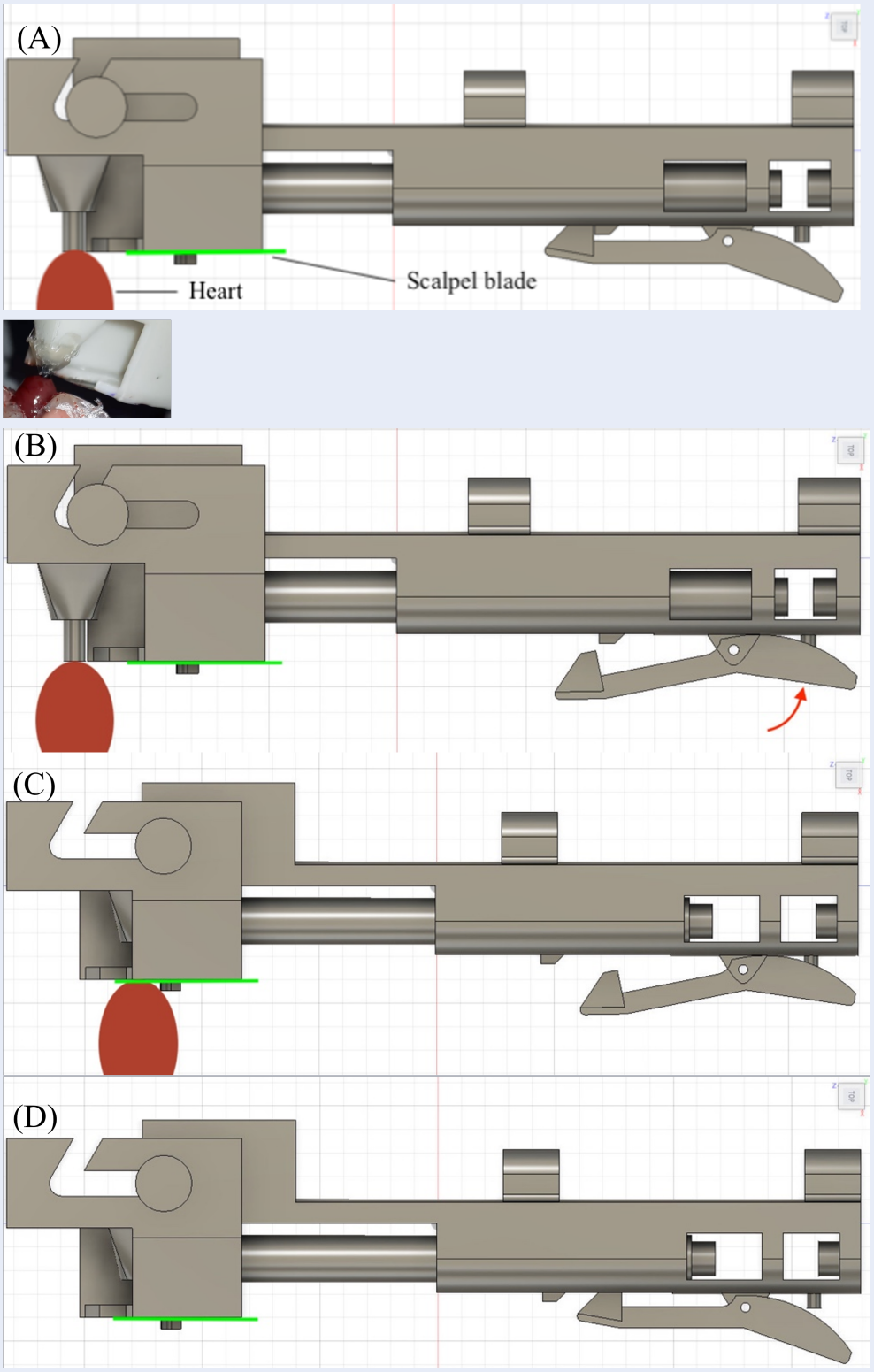

Figure 14: **Motion demonstration of the negative pressure cutter**. (A) the cutter is pushed to the left into the compress position. (B) The release of the latch occurs when force is applied to the trigger located at the arrow position. (C) The spring exerts a force on the latch and the cutter, causing them to move in the leftward direction. (D) The trigger undergoes a return to its initial position at high velocity and performs the cutting.

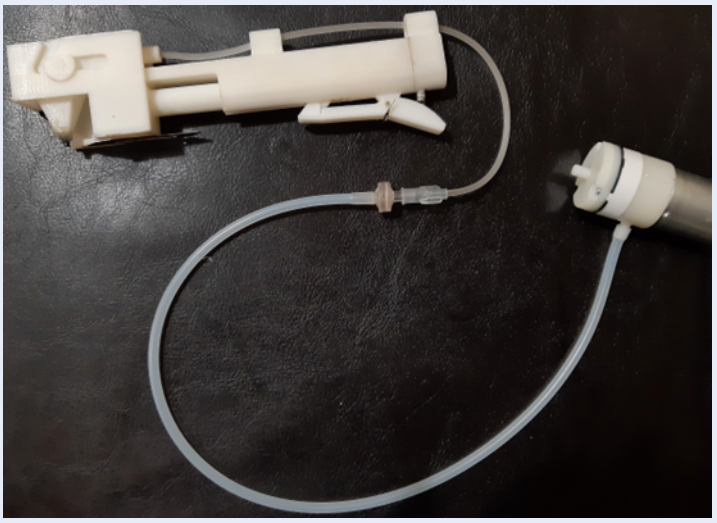

Figure 15: **Demonstration of the final prototype of the cutter including vacuum pump, connecting tube, regulating valve, and the device.**

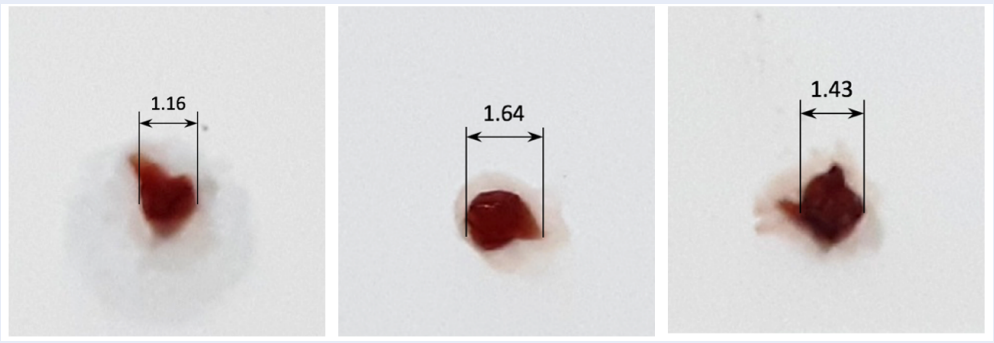

Figure 16: **Depiction of cutting samples with 1.16 mm, 1.64 mm, 1.43 mm**. A camera was utilized to capture a total of sixteen samples, each of which was accompanied by a calibration ruler for reference purposes.

of 16. The obtained p-value is 0.474. Based on the Shapiro-Wilk test results, it can be concluded that the calculated p-value is greater than the predetermined significance level of 0.05. This suggests that the observed distribution is consistent with the assumption of normality.

DISCUSSION

Early negative pressure cutters (**Figure 19**) had the suction head integrated into the main construction and were 3D printed along with other elements. Layer-by-layer 3D printing causes airtightness issues in the finished goods. Air leakage from the suction head across the main body has reduced suction force. The current version fixes this by connecting the suction head and tiny vacuum pump with a closed, airtight connection. This adjustment boosts negative pressure, thus allowing the blade to pierce dense and tough cardiac tissue, unlike prior generations.

The scalpel blade incision started cardiac apex morphological change. Air pressure is disrupted by this change, affecting the heart-suction head contact surface stability. The heart's apex tends to disengage from the suction head during stability interruptions, elongating the "tail". 3D printed items with rough surfaces increase friction between moving parts, causing sample variance. To reduce friction during operation, component joints must be spaced apart. The heart's connective tissue layers are highly resistant to rupture[42]; therefore, blade selection should be done carefully. A razor blade was used to start the experiment since its thinness makes it easy to fragment. However, in tough tissues like heart muscle, razor blades are ineffective for cutting. During testing, the blade

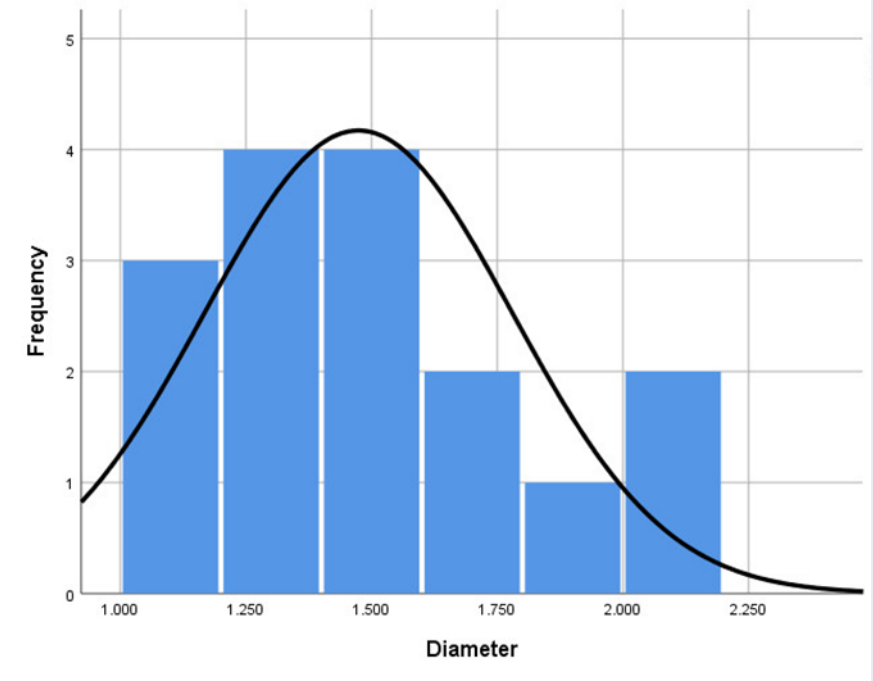

Figure 17: **Histogram distribution of the dataset. The mean value ( ) is 1.4736 millimeters, and the standard deviation (s) is 0.306 millimeters**. By employing the One-sample T-test, the 95% confidence interval for the difference yields that the lower bound is 1.3106 millimeters, and the upper bound is 1.6367 millimeters.

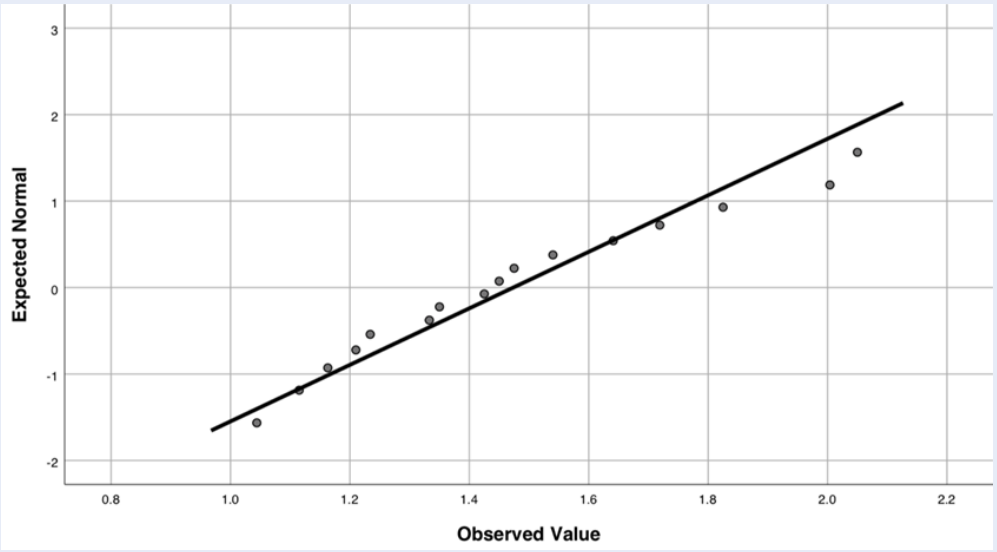

Figure 18: **Illustration of the presence of skewness in the cut sample diameter dataset with normal Q-Q plot**. The skewness statistic of 0.563 inferred that the distribution is rightward skewed and has a moderate positive skew.

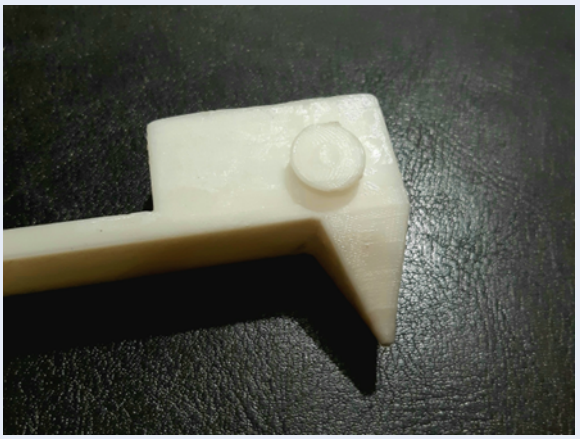

Figure 19: **The previous version of the negative pressure cutter**. The vacuum head, along with other components, was 3D printed and integrated into the main structure. Layer-by-layer 3D printing compromises the airtightness of the final product. Due to air leakage across the main body from the suction tip, the suction force is diminished.

often moved from its cutting point, sometimes causing slight cardiac tissue abrasion and displacing the heart from the suction apparatus. The surgical scalpel blade, being sharper than the razor blade, allows it to penetrate the heart apex; however, it still cuts poorly, leaving a "tail". Thus, cutting velocity, angle, and suction force must be studied to improve cutting results. The principal experiment's suction head was made by removing the sharp end of a veterinary needle, which has an inner diameter of 0.838 mm. The experimental results suggest that this needle is unsuitable for this study. Scalpel blades can only make superficial incisions and displace the heart. Metallic nozzles produce poor results as the firm and polished metal surface make vacuum heads hard to close. Following this finding, a plastic tube was used to make the nozzle. The elastic and surface qualities of plastic make contact more stable, increasing suction force. This ensures the cutting process is exact and meets specifications. However, the above cutting outcomes show that a residual "tail" deviates from the expected cutting pattern. To improve cutting results, experimentation with different nozzle diameters and suction pressure levels is necessary to find the best setup.

The variability in cut size seen in our study has significant implications for the research results and possible beneficial uses of our device. This variation might be ascribed to many aspects, such as tissue characteristics and cutting parameters, which require careful attention for interpreting our results and developing future applications. From our viewpoint, variations in tissue characteristics like density, flexibility, and composition can impact the efficiency of tissue removal. Different tissues may react distinctively to cutting forces, resulting in variations in the size of the cut. Blade sharpness, cutting speed, and cutting angle are attributes that can affect the accuracy and uniformity of tissue removal. Using inadequate cutting criteria can lead to inconsistent or inadequate cuts, causing variations in the size of the cuts. It is essential to comprehend the factors that influence the variation in cut size to enhance the efficiency of our devices and experimental procedures. Identifying and resolving these parameters would enhance the precision and consistency of apical resection in neonatal mouse hearts, thereby improving the validity of our research outcomes. Our research establishes a foundation for refining cutting techniques and device design to obtain more consistent and predictable tissue resection outcomes by examining the relationship between tissue characteristics, cutting parameters, and cut size variability.

Challenges arose during the design and testing stages of our 3D-printed negative pressure cutter, which warrant further investigation. One major obstacle was fine-tuning the negative pressure system to guarantee accurate management of tissue stability while cutting. Fluctuations in negative pressure levels and the risk of leakage hindered the attainment of consistent and dependable outcomes. To address this challenge, we intend to investigate innovative methods of pressure regulation and enhance the suction head's design to improve sealing and reduce air leakage. Furthermore, including real-time monitoring and feedback systems into the device could improve regulation

and reduce the effects of variations in negative pressure.

The initial investigation's lack of thorough statistical analysis restricted the strength of our conclusions and the applicability of the device's effectiveness[43]. In the future, we aim to perform more thorough statistical analyses, such as comparing studies with current methods and the incorporation of control groups, to offer more compelling evidence for the device's effectiveness and dependability. Increasing the sample size and including longitudinal research will improve the statistical power and validity of our results, allowing for more reliable conclusions.

To enhance the design and functionality of our 3D-printed negative pressure cutter for apical excision in neonatal mouse hearts, we will tackle these problems and employ ways to overcome constraints. We aim to enhance the field of cardiac regenerative medicine and surgery through ongoing research and development, ultimately leading to better outcomes for patients with heart disease.

CONCLUSION AND FUTURE WORKS

In summary, this study created and tested a 3D-printed negative pressure cutter for neonatal mouse heart apical excision. It addressed the issues of irregular sample cuts and the lack of specialized cutting devices in the research field.

Successfully developing the proposed device required iterative design approaches. Advanced features, including an automated cutter, a negative pressure system, and a suction head, provided precise and controlled resections. The device achieved precise sample cuts with a clean, uncontaminated resection surface while being compact and portable for laboratory use.

Although limited by a somewhat larger sample size than expected, the trial results revealed the device's operational efficacy. Despite exceeding the desired diameter of 1 millimeter by a small margin, the stability of the resultant diameter showed promising advances in cutter optimization for apical resection in neonatal mouse hearts.

The study also examined design factors such as securing the heart apex during cutting, establishing protocols to ensure consistent sample diameters, selecting appropriate blade shapes, and optimizing the resection method to reduce human errors. This technology addressed these problems by providing a reliable and automated cutting mechanism that improved accuracy and reduced variability.

The study has provided useful insights into the development and initial evaluation of the 3D-printed negative pressure cutter for apical excision in neonatal mouse hearts. However, we recognize limitations related to sample size and statistical analysis. In the future, we will focus on addressing these deficiencies to enhance the quality and dependability of our research. We aim to increase the size of our study cohort in future research to address the restriction posed by the limited sample size. To enhance the statistical strength of our findings and achieve better representation and heterogeneity within the population of neonatal mice, we plan to increase the sample size. This enlargement will enable more comprehensive conclusions and wider applicability of the device's effectiveness and dependability under different experimental conditions.

In addition, we intend to include more advanced statistical tests in our future studies to overcome the lack of thorough statistical analysis. These may include conducting analysis of variance (ANOVA), comparative research with current procedures, and incorporating control groups or comparisons with manual resection techniques. We will enhance the data supporting the performance of the 3D-printed negative pressure cutter through a more thorough statistical analysis and provide a definitive baseline for assessing its benefits.

We acknowledge the wider ramifications of our research and the potential for future endeavors, in addition to addressing the current issues. One way to enhance the credibility and accuracy of our device is by working with other researchers or institutions to validate and improve it. By utilizing the knowledge and resources of partners, we can strengthen the quality of our study and explore potential uses of the device in fields like tissue engineering and developmental biology.

ABBREVIATIONS

3D: 3 dimensions, **Q-Q**: Quantile-Quantile.

ACKNOWLEDGMENTS

None.

AUTHOR'S CONTRIBUTIONS

Conceptualization, Ngoc-Bich Le, Thi-Thu-Hien Pham; methodology, Ngoc-Bich Le, Thi-Thu-Hien Pham, Minh-Thu Le; validation, Thanh-Hai Le; formal analysis, Ngoc-Bich Le, Thanh-Hai Le; investigation, Ngoc-Bich Le, Thi-Thu-Hien Pham, Minh-Thu Le; data curation, Minh-Thu Le; writing - original draft preparation, Ngoc-Bich Le, Minh-Thu Le; writing review and editing, Thi-Thu-Hien Pham, Quoc-Hung Phan; supervision, Ngoc-Bich Le, Thi-Thu-Hien Pham; funding acquisition, Van-Toi

Vo. All authors have read and agreed to the published version of the manuscript.

FUNDING

This research was funded by Vietnam National University Ho Chi Minh City (VNU-HCM) under Grant No. NCM2020–28-01.

AVAILABILITY OF DATA AND MATERIALS

Data and materials used and/or analyzed during the current study are available from the corresponding author on reasonable request.

ETHICS APPROVAL

The research outlined in this paper demonstrates a commitment to upholding the utmost ethical standards in the handling and utilization of animals. The experimental procedures carried out on neonatal mice adhered to the guidelines and regulations established by the ethical review boards and institutions responsible for overseeing animal research. Prior to the commencement of the research, the study protocol and experimental procedures underwent a thorough review and received approval (i.e. approval number: A_2022_J1/HHĐĐ – K. KTYS/ĐHQT) from the relevant ethics committee review board.

The study also emphasized the application of the 3Rs principle (Replacement, Reduction, and Refinement) in the context of animal research. Efforts were made to substitute animal models with alternative methodologies whenever feasible, with the aim of reducing the overall utilization of animals and improving animal welfare by refining experimental techniques to mitigate potential harm.

CONSENT FOR PUBLICATION

Not applicable.

COMPETING INTERESTS

The authors declare that they have no competing interests.

REFERENCES

1. Carotenuto F, Teodori L, Maccari AM, Delbono L, Orlando G, Nardo PD. Turning regenerative technologies into treatment to repair myocardial injuries. Journal of Cellular and Molecular Medicine. 2020;24(5):2704–16. PMID: 31568640. Available from: https://doi.org/10.1111/jcmm.14630.
2. Meng WT, Guo HD. Small Extracellular Vesicles Derived from Induced Pluripotent Stem Cells in the Treatment of Myocardial Injury. International Journal of Molecular Sciences. 2023;24(5):4577. PMID: 36902008. Available from: https://doi.org/10.3390/ijms24054577.
3. Shao CL, Cui GH, Guo HD. Effects and Mechanisms of Taohong Siwu Decoction on the Prevention and Treatment of Myocardial Injury. Frontiers in Pharmacology. 2022;13:816347. PMID: 35153789. Available from: https://doi.org/10.3389/fphar.2022.816347.
4. Zhao T, Wu W, Sui L, Huang Q, Nan Y, Liu J. Reactive oxygen species-based nanomaterials for the treatment of myocardial ischemia reperfusion injuries. Bioactive Materials. 2021;7:47–72. PMID: 34466716. Available from: https://doi.org/10.1016/j.bioactmat.2021.06.006.
5. Luo T. Treatment with metformin prevents myocardial ischemia-reperfusion injury via STEAP4 signaling pathway. Anatolian Journal of Cardiology/Anadolu Kardiyoloji Dergisi. 2019;21(5):11456. Available from: https://doi.org/10.14744/AnatolJCardiol.2019.11456.
6. Rostamzadeh F, Najafipour H, Aminizadeh S, Jafari E. Therapeutic effects of the combination of moderate-intensity endurance training and MitoQ supplementation in rats with isoproterenol-induced myocardial injury: the role of mitochondrial fusion, fission, and mitophagy. Biomedicine and Pharmacotherapy. 2024;170:116020. PMID: 38147733. Available from: https://doi.org/10.1016/j.biopha.2023.116020.
7. Wang S, Chen Y, Wu C, Wang Y, Lin W, Bu R. Trehalose Alleviates Myocardial Ischemia/Reperfusion Injury by Inhibiting NLRP3-Mediated Pyroptosis. Applied Biochemistry and Biotechnology. 2023;196(3):1194–210. Available from: https://doi.org/10.1007/s12010-023-04613-8.
8. Yang P, Liu M, Fan X, Zhang X, Cao L, Wang Z. Recent Advances in Natural Plant-based Treatment of Myocardial Ischemia-reperfusion Injury. International Journal of Drug Discovery and Pharmacology. 2023;21:21. Available from: https://doi.org/10.53941/ijddp.2023.100003.
9. Tripathi P, Biotechnol Kiosk. Applications of Omics Technologies in Regenerative Therapies for Cardiac Repair. 2021;3(6):3–12. Available from: https://doi.org/10.37756/bk.21.3.6.1;https://biotechkiosk.com/wp-content/uploads/2022/04/Perspective_June2021.pdf.
10. Park M, Yoon YS. Cardiac Regeneration with Human Pluripotent Stem Cell-Derived Cardiomyocytes. Korean Circulation Journal. 2018;48(11):974–88. PMID: 30334384. Available from: https://doi.org/10.4070/kcj.2018.0312.
11. Lee CS, Kim J, Cho HJ, Kim HS. Cardiovascular Regeneration via Stem Cells and Direct Reprogramming: A Review. Korean Circulation Journal. 2022;52(5):341–53. PMID: 35502566. Available from: https://doi.org/10.4070/kcj.2022.0005.
12. Minguell JJ, Erices A. Mesenchymal stem cells and the treatment of cardiac disease. Experimental Biology and Medicine (Maywood, NJ). 2006;231(1):39–49. PMID: 16380643. Available from: https://doi.org/10.1177/153537020623100105.
13. Le TY, Thavapalachandran S, Kizana E, Chong JJ. New Developments in Cardiac Regeneration. Hear Lung and Circulation. 2017;26(4):316–22. Available from: https://doi.org/10.1016/j.hlc.2016.11.002.
14. Gara E, Kosztin A, Harding SE, Földes G. Stem Cell Therapy to Treat Heart Failure. Comprehensive Biotechnology. 2019;5:286–303. Available from: https://doi.org/10.1016/B978-0-444-64046-8.00302-5.
15. Hénon P. Key Success Factors for Regenerative Medicine in Acquired Heart Diseases. Stem Cell Reviews and Reports. 2020;16(3):441–58. PMID: 32297205. Available from: https://doi.org/10.1007/s12015-020-09961-0.
16. Bartunek J, Terzic A, Davison BA, Behfar A, Sanz-Ruiz R, Wojakowski W, et al. Cardiopoietic stem cell therapy in ischaemic heart failure: long-term clinical outcomes. ESC Heart Failure. 2020;7(6):3345–54. Available from: https://doi.org/10.1002/ehf2.13031.
17. Rumyantsev PP. Autoradiographic study on the synthesis of DNA, RNA, and proteins in normal cardiac muscle cells and those changed by experimental injury. Folia Histochemica et Cytochemica. 1966;4(4):397–424. PMID: 5959688.
18. Witman N, Murtuza B, Davis B, Arner A, Morrison JI. Recapitulation of developmental cardiogenesis governs the morphological and functional regeneration of adult newt hearts following injury. Developmental Biology. 2011;354(1):67–76.

PMID: 21457708. Available from: https://doi.org/10.1016/j.ydbio.2011.03.021.
19. Drenckhahn JD, Schwarz QP, Gray S, Laskowski A, Kiriazis H, Ming Z. Compensatory growth of healthy cardiac cells in the presence of diseased cells restores tissue homeostasis during heart development. Developmental Cell. 2008;15(4):521–33. PMID: 18854137. Available from: https://doi.org/10.1016/j.devcel.2008.09.005.
20. Li F, Wang X, Capasso JM, Gerdes AM. Rapid transition of cardiac myocytes from hyperplasia to hypertrophy during postnatal development. Journal of Molecular and Cellular Cardiology. 1996;28(8):1737–46. PMID: 8877783. Available from: https://doi.org/10.1006/jmcc.1996.0163.
21. Walsh S, Pontén A, Fleischmann BK, Jovinge S. Cardiomyocyte cell cycle control and growth estimation in vivo—an analysis based on cardiomyocyte nuclei. Cardiovascular Research. 2010;86(3):365–73. PMID: 20071355. Available from: https://doi.org/10.1093/cvr/cvq005.
22. Kikuchi K, Poss KD. Cardiac regenerative capacity and mechanisms. Annual Review of Cell and Developmental Biology. 2012;28(1):719–41. PMID: 23057748. Available from: https://doi.org/10.1146/annurev-cellbio-101011-155739.
23. Porrello ER, Mahmoud AI, Simpson E, Johnson BA, Grinsfelder D, Canseco D. Regulation of neonatal and adult mammalian heart regeneration by the miR-15 family. Proceedings of the National Academy of Sciences of the United States of America. 2013;110(1):187–92. PMID: 23248315. Available from: https://doi.org/10.1073/pnas.1208863110.
24. Rui L, Yu N, Hong L, Feng H, Chunyong H, Jian M. Extending the time window of mammalian heart regeneration by thymosin beta 4. Journal of Cellular and Molecular Medicine. 2014;18(12):2417–24. PMID: 25284727. Available from: https://doi.org/10.1111/jcmm.12421.
25. Zlatanova I, Pinto C, Bonnin P, Mathieu JR, Bakker W, Vilar J. Iron Regulator Hepcidin Impairs Macrophage-Dependent Cardiac Repair After Injury. Circulation. 2019;139(12):1530–47. PMID: 30586758. Available from: https://doi.org/10.1161/CIRCULATIONAHA.118.034545.
26. Cai B, Ma W, Wang X, Sukhareva N, Hua B, Zhang L. Targeting LncDACH1 promotes cardiac repair and regeneration after myocardium infarction. Cell Death and Differentiation. 2020;27(7):2158–75. PMID: 31969690. Available from: https://doi.org/10.1038/s41418-020-0492-5.
27. Hu L, Liang M, Jiang Q, Jie Y, Chen L, Zhang F. Proteomic analysis of neonatal mouse hearts shows PKA functions as a cardiomyocyte replication regulator. Proteome Science. 2023;21(1):16. PMID: 37821903. Available from: https://doi.org/10.1186/s12953-023-00219-4.
28. Ahmed A, Wang T, Delgado-Olguin P. Ezh2 is not required for cardiac regeneration in neonatal mice. Plos one. 2018;13(2):e0192238. Available from: https://doi.org/10.1371/journal.pone.0192238.
29. Polizzotti BD, Ganapathy B, Walsh S, Choudhury S, Ammanamanchi N, Bennett DG, et al. Neuregulin stimulation of cardiomyocyte regeneration in mice and human myocardium reveals a therapeutic window. Science Translational Medicine. 2015;7(281):281ra45. PMID: 25834111. Available from: https://doi.org/10.1126/scitranslmed.aaa5171.
30. Ganapathy B, Nandhagopal N, Polizzotti BD, Bennett D, Asan A, Wu Y, et al. Neuregulin-1 administration protocols sufficient for stimulating cardiac regeneration in young mice do not induce somatic, organ, or neoplastic growth. PloS one. 2016;11(5):e0155456.
31. Haubner BJ, Schuetz T, Penninger JM. A reproducible protocol for neonatal ischemic injury and cardiac regeneration in neonatal mice. Basic Research in Cardiology. 2016;111(6):64. PMID: 27665606. Available from: https://doi.org/10.1007/s00395-016-0580-3.
32. Xiong J, Hou J. Apical resection mouse model to study early mammalian heart regeneration. Journal of Visualized Experiments. 2016;107:e53488.
33. Polizzotti BD, Ganapathy B, Haubner BJ, Penninger JM, Kühn B. A cryoinjury model in neonatal mice for cardiac translational and regeneration research. Nature Protocols. 2016;11(3):542–52. PMID: 26890681. Available from: https://doi.org/10.1038/nprot.2016.031.
34. Porrello ER, Mahmoud AI, Simpson E, Hill JA, Richardson JA, Olson EN, et al. Transient regenerative potential of the neonatal mouse heart. Science. 2011;331(6020):1078–80. Available from: https://doi.org/10.1126/science.1200708.
35. Li Y, Feng J, Li Y, Hu S, Nie Y. Achieving stable myocardial regeneration after apical resection in neonatal mice. Journal of Cellular and Molecular Medicine. 2020;24(11):6500–4. PMID: 32343038. Available from: https://doi.org/10.1111/jcmm.15223.
36. Liu Y, Wang H, Zhang H, Wang J, Liu Q, Bi Y. CUGBP1, a crucial factor for heart regeneration in mice. Cell Death {&}amp; Disease. 2022;13(2):120. PMID: 35136022. Available from: https://doi.org/10.1038/s41419-022-04570-w.
37. Hegde SM. Pericardial Disease. In: Essential Echocardiography. Elsevier; 2019. p. 347-353.e1. 2019;Available from: https://doi.org/10.1016/B978-0-323-39226-6.00033-3.
38. Jaworska-Wilczynska M, Trzaskoma P, Szczepankiewicz AA, Hryniewiecki T. Pericardium: structure and function in health and disease. Folia Histochemica et Cytobiologica. 2016;54(3):121–5. PMID: 27654013. Available from: https://doi.org/10.5603/FHC.a2016.0014.
39. Mahmoud AI, Porrello ER, Kimura W, Olson EN, Sadek HA. Surgical models for cardiac regeneration in neonatal mice. Nature Protocols. 2014;9(2):305–11. PMID: 24434799. Available from: https://doi.org/10.1038/nprot.2014.021.
40. Han C, Nie Y, Lian H, Liu R, He F, Huang H. Acute inflammation stimulates a regenerative response in the neonatal mouse heart. Cell Research. 2015;25(10):1137–51. PMID: 26358185. Available from: https://doi.org/10.1038/cr.2015.110.
41. Davidovits P. Physics in Biology and Medicine. third. Amsterdam: Elsevier/Academic Press; 2008. . 2008;.
42. Paneitz DC, Vlahakes GJ. Surgical Anatomy of the Heart. InCardiac Surgery Clerkship: A Guide for Senior Medical Students 2024 Jan 25 (pp. 13-25). Cham: Springer International Publishing;Available from: https://doi.org/10.1007/978-3-031-41301-8_2.
43. Dwivedi AK, Shukla R. Evidence based statistical analysis and methods in biomedical research (SAMBR) checklists according to design features. Cancer Reports. 2020;3(4):e1211. Available from: https://doi.org/10.1002/cnr2.1211.